*Geopersia* ***10*** *(1), 2020, PP. 149-163* *DOI: 10.22059/GEOPE.2019.284414.648488*

# A clustering approach for mineral potential mapping: A deposit–scale porphyry copper exploration targeting

**Mohammad Javad Rezapour, Maysam Abedi*, Abbas Bahroudi, Hossain Rahimi**
*Geo–Exploration Targeting Lab (GET–Lab), School of Mining Engineering, College of Engineering, University of Tehran, Iran.*
**Corresponding author, e–mail: maysamabedi@ut.ac.ir*
(*received: 28/06/2019 ; accepted: 03/11/2019*)

**Abstract**

This work describes a knowledge–guided clustering approach for mineral potential mapping (MPM), by which the optimum number of clusters is derived form a knowledge–driven methodology through a concentration–area (C–A) multifractal analysis. To implement the proposed approach, a case study at the North Narbaghi region in the Saveh, Markazi province of Iran, was investigated to discover porphyry Cu–bearing favorability zones. Whereby, various exploratory indicators were extracted from a multidisciplinary geospatial data set comprising of geology, geophysics and geochemistry criteria. Those indicators were prepared from magnetometry and geo–electrical survey, lithogeochemical samples and geological field operation. The optimum number of clusters was obtained by running the knowledge–based methods of index overlay and fuzzy gamma operators, indicating five clusters from the C–A multifractal curve. Accessing to exploratory drilling lets us to find out the most efficient synthesized favorability map that was generated by a fuzzy algebraic sum operator (or a gamma value equal to one). Assuming the optimum number of clusters, three clustering methods, namely fuzzy C–means (FCM), K–means and self–organizing map were examined for MPM. Note that the FCM as an unsupervised data–driven methodology, had superiority over other clustering analyses by generating mineral favorability map in close association with drilling results.

**Keywords**: *Mineral Potential Mapping, Index Overlay, Fuzzy Gamma Operator, Clustering.*

## Introduction

Mineral potential mapping (MPM) is a sophisticated geospatial data processing and integration task, by which a district/deposit scale region is delimited into some favorable potential zones to detect ore mineralization targets with higher certainty. For achieving this aim, one of the important steps is accessibility to a multidisciplinary and high quality geospatial data set in which data are powerful footprints of sought mineral target (Abedi *et al.,* 2013a,b). According to the type of sought mineral target, various exploratory criteria, namely geology, remote sensing, geochemistry and geophysics are taken into account. Therefore, if indicator layers extracted from exploratory criteria are quantified correctly, synthesized indicators presenting mineral favorability zones will be reliable (Carranza, 2008).

Utilizing a variety of available exploratory data and maps, and the capabilities of the geographical information system (GIS), an MPM can easily be generated to reveal the most probabilistic locations in terms of favorability for unknown ore occurrences (Carranza, 2008). Therefore, several exploratory indicators are generated to integrate and analyze synthesized favorability maps ( Najafi *et al.,* 2014; Yousefi & Carranza, 2015a, b; Kashani *et al.,* 2016). An exploration information system has been also suggested as a new idea for an information system to better integrate the conceptual mineral deposit model with available data set to support exploration targeting and discuss how best to categorize a mineral system as scale–dependent subsystem to form a mineral deposit (Yousefi *et al.,* 2019).

Different MPM methodologies have been developed in the last two decades, which in general can be divided into three main categories (Pan & Harris, 2000; Carranza, 2008; Kashani *et al.,* 2016). Methods of data integration are categorized into (1) knowledge–driven, (2) data–driven, and (3) hybrid approaches.

In supervised data–driven methods, known mineral deposits are used as "training points" to create spatial relationships with specific geological, geochemical and geophysical features (Carranza, 2008; Kashani *et al.,* 2016). Relationships are quantified to assign a weight of importance for each indicator on the basis of a computational algorithm (Carranza & Hale, 2002a; Kashani *et al.,* 2016), and ultimately those indicators are integrated into a single mineral favorability map ( Nykänen & Salmirinne, 2007; Kashani *et al.,* 2016). Examples of data–driven methods are logistic regression (Agterberg & Bonham–Carter, 1999; Carranza & Hale, 2001; Mejía–Herrera *et al.,* 2015), neural

networks (Singer & Kouda, 1996; Porwal *et al.,* 2003, 2004; Harris *et al.,* 2003; Nykänen, 2008; Abedi & Norouzi, 2012;), weights of evidence (Bonham–Carter, 1989; Agterberg *et al.,* 1990; Carranza & Hale, 2002b), support vector machine (Abedi & Norouzi, 2012; Shabankareh & Hezarkhani, 2017), and random forests (Carranza & Laborte, 2016; Zhang *et al.,* 2016). Unsupervised data–driven methods (without needing to training points) are clustering algorithms which divide multidimensional feature space into some clusters (Paasche & Eberle, 2009; Eberle & Paasche, 2012; Abedi *et al.,* 2013b).

Another main group for MPM is knowledge–driven methods, which are based on a geoscientists' opinions (Abedi *et al.,* 2013a,b; Kashani *et al.,* 2016). They are Boolean logic (Bonham–Carter, 1989, 1994; Abedi *et al.,* 2013b), index overlay (Bonham–Carter, 1994; Carranza *et al.,* 1999; Abedi *et al.,* 2013b; Mirzaei *et al.,* 2014; Sadeghi *et al*., 2014; Sadeghi & Khalajmasoumi, 2015), fuzzy logic (An *et al*., 1991; Chung & Moon, 1991; Abedi et al., 2013c; Moradi *et al.,* 2015; Sadeghi & Khalajmasoumi, 2015; Kashani *et al.,* 2016), outranking methods (Abedi *et al.,* 2012a,b; Abedi *et al.,* 2013a; Abedi *et al.,* 2015), and evidential belief functions (Moon, 1990; Tangestani & Moore, 2002). Hybrid algorithms are also a combinatory of knowledge– and data–driven methods, where simultaneous consideration of both approaches are taking into consideration (Porwal *et al.,* 2003, 2004; Pazand & Hezarkhani, 2015).

Despite three main groups of MPM, two novel approaches have been proposed to outperform synthesized mineral favorability maps that are (a) a hybrid algorithm by simultaneous consideration of both locations of known mineral occurrences and expert attitudes, and (2) weighting to the continuous spatial evidence without consideration of the location of known mineral occurrences and expert judgments (Yousefi & Carranza 2015c, 2016a, b).

Among data–driven methods, unsupervised algorithms of clustering have been rarely applied in MPM. One reason can be related to unknown number of clusters which has substantial effect on the final synthesized mineral favorability map. Correct determination of the cluster number has been investigated in several field of studies (e.g. Rajabinasab & Asghari 2019). This work has examined a knowledge–guided clustering methodology, where the optimum number of clusters is determined on the basis of multifractal characteristics of a knowledge–driven mineral favorability map in association with the geological setting of a prospect zone. Index overly and fuzzy gamma operators are employed here to integrate indicator layers, and subsequently mineral favorability maps are divided into some clusters. The cluster number is defined to run fuzzy C–means (FCM), K–means (KM) and self–organizing map (SOM) algorithms. On the basis of drilling results, the FCM clustering could efficiently localize two separate zones in association with porphyry copper mineralization at the North Narbaghi prospect zone in Saveh, Markazi province of Iran. A deposit–scale MPM in porphyry ore mineralization system usually utilizes several types of exploratory data that are geophysical evidences derived from magnetometry and geo–electrical surveys, geological evidences from the geological data set (i.e. lithology, lineament and alteration), and geochemical evidences (Abedi *et al.,* 2017).

The remainder of this research has been prepared as follows. Geological setting of the North Narbaghi porphyry copper mineralization is explained in the second section. Geospatial dataset is constructed in the third section, where a multidisciplinary database is designed from geophysical (magnetometry and geo–electrical data), geological and geochemical surveys. In fourth section, indicator layers are integrated through a knowledge–guided clustering algorithm. Then in fifth section, the performance and quality of generated mineral favorability maps are discussed by comparison to the geometry of the main source of Cu mineralization. Finally, main achievements are summarized in the conclusion.

## Geological setting of the North Narbaghi Cu mineralization

From the geological point of view, the North Narbaghi Cu deposit as a type of volcano–genetic mineralization, is located on the volcanic belt of the Urmia–Dokhtar magmatic assemblage (UDMA) in the structural geology divisions of Iran (Ramazi & Jalali, 2015). This volcanic belt, shown in Fig. 1a, is classified as an Andean–type magmatic arc due to the closure of the Neo–Tethys ocean between the Arabian plate and the Eurasian plate (Shahabpour, 2005; Kazemi *et al.,* 2019). The Saveh district is located at the UDMA zone, as the main host of the porphyry deposits such as Cu, Au and Mo in Iran (Berberian & King, 1981; Rezaei *et al.,* 2015). The main rock units dominated the North Narbaghi have

been summarized in three main groups as following:

(1) Monzogranite to quartz monzonite units hosted the most Cu mineralized regions, severely dominated by argillic alteration (Fig. 2a). The number of magmatic intrusions in the region is somewhat high, where most portions were exposed in small sizes. The age of these masses is equivalent to the early Oligocene. The structural lineaments of the region have substantially controlled the deployment of such magmatic intrusions since most intrusive sources in adjacency to the Saveh were manifested on the margins of the lineaments. Therefore, such phenomena could be in association with a batholith source as the feeder of the intrusive masses in this region. Two types of hydrothermally alteration were visible in this unit. Phyllic alteration occurred in portions with minerals of pyrite, sericite and quartz. In addition, over areas with depletion of the Cu mineralization, the argillic alteration has severely affected the rocks. Meanwhile, the intrusive units were intact and unaltered in some portions as well.

(2) Basaltic andesite rocks with a distinct silicic alteration. Volcanic activities in the North Narbaghi copper deposit led to the generation of the basaltic andesite unit within the porphyritic hornblende andesite rocks (Fig. 2b), with a dark gray color and a distinct outcrop than the surrounding rocks. These rocks were mostly surrounded by the monzogranite and quartz monzodiorite units.

(3) Porphyritic hornblende andesite units affected by the hydrothermally propylitic alteration have surrounded the mineralized Cu zones (Fig. 2c). Intense alteration of coarse crystals namely chlorite, epidote and carbonate has appeared in the andesite unit, leading to the transformation of plagioclase and amphibole into such minerals. Moreover, the andesine rock, as the oldest unit with an Eocene age and the most extensive rock, occurred in the south of the North Narbaghi.

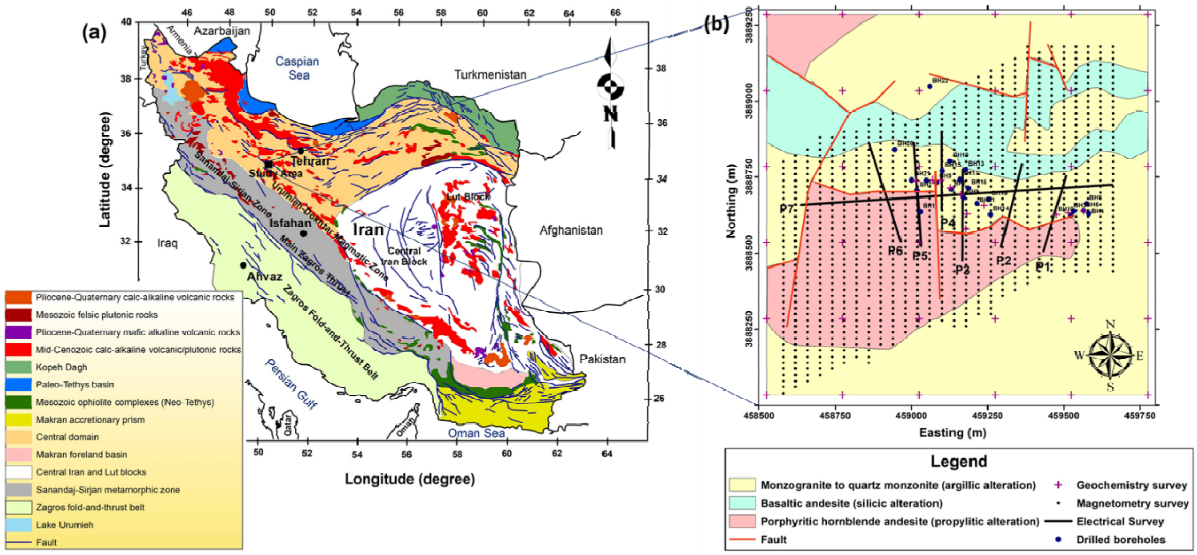


Figure 1. The general geological setting of Iran (a), the simplified geological units in the North Narbaghi copper deposit and the alteration map (b).


Figure 2. Sample photos of the main rock units in the North Narbaghi, (a) monzogranite to quartz monzonite, (b) basaltic andesite, and (c) porphyritic hornblende andesite (Dehghan Nayeri 2018).

Chlorite alteration was also sporadically visible in some portions and its intensity has increased in adjacency to the mineralized regions (Ghalamghash, 1998; Ramazi & Jalali, 2015).

Structural lineaments (i.e. faults, fractures and contacts) with few traces in the area had low impact on the Cu mineralization. The disseminated type of the Cu mineralization was not strongly in association with the structural lineaments, while the effect of the faults just led to partially Cu enrichment. The largest fault trace was observed in the west portion of the studied region with an approximate north–south trend (Dehghan Nayeri, 2018).

**Geospatial data set**

In the following sub–sections, seven indicator layers from geological, geochemical, and geophysical data are extracted to construct a multidisciplinary geospatial database. A decision matrix with 9136 rows of data points and 7 columns of indicators was constructed to synthesize mineral favorability maps. Processing of each indicator was such that each layer lies at an interval from 0 to 1 to suppress perturbation effect arising from different data scales.

*Geological layers*

Due to the presence of the main host rocks of Cu mineralization in the region, the monzogranite to quartz monzonite units were assigned the highest score by expert decision makers (DMs). The importance of other rocks with lower impact on ore mineralization was reflected in the rock type indicator layer (Fig. 3a). In addition, since phyllic alteration has occurred in regions with higher enrichment of Cu–bearing mineralization, the highest score was assumed for this attribute in the alteration indicator layer. The lowest score is considered for the propylitic alteration, which surrounds the main regions of mineralization. The importance of alteration system in the porphyry type Cu mineralization was taken into account as the second geological indicator layer (Fig. 3b). Since there were no traces of copper mineralization in association with the fault activities in the North Narbaghi, this layer was not involved in the exploratory decision matrix.

*Geochemical layers*

Totally, 47 lithogeochemical samples were collected systematically with a regular grid distance of 250 m over the North Narbaghi. The sampling distance reduced to 50 m over the monzogranite and quartz monzonite units where there were sharp geological evidences of the Cu mineralization. The normalized map of the Cu concentration as a geochemical indicator layer is shown in Fig. 4a. To investigate spatially correlation among concentration of analyzed elements, the descriptive statistical characteristics of the main eight elements correlated with Cu are presented in Table 1. The Pearson's linear correlation coefficient for six elements of Mo, Zn, Co, As, Sb and Li against the Cu concentration is tabulated in Table 2. These positive correlations were only negative for Mg element (–0.567), where depletion has occurred in the mineralized zones.

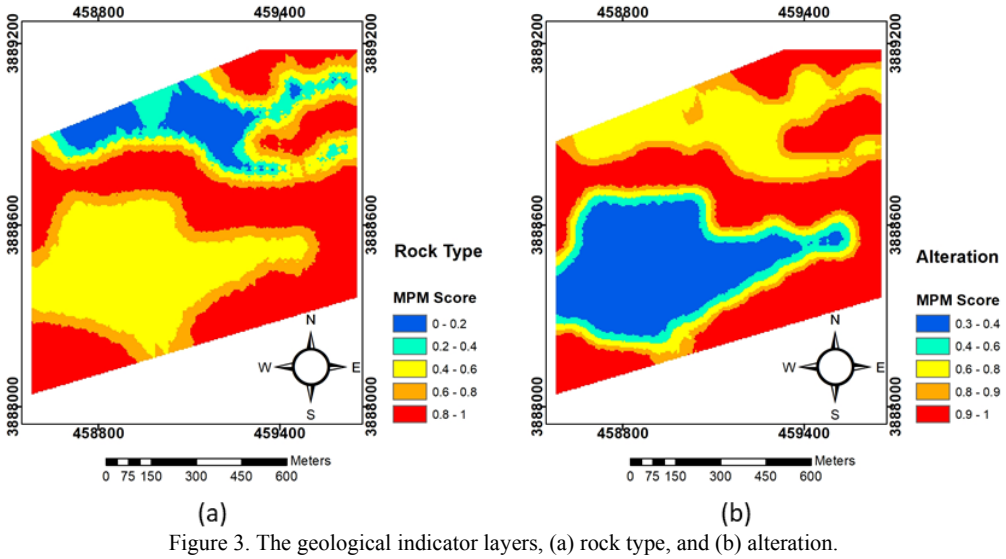


Figure 3. The geological indicator layers, (a) rock type, and (b) alteration.

Table 1. Descriptive Statistical summaries of main correlated elements (in ppm)

| Element | Min | Max | Mean | Median | Std. | Skewness | Kurtosis |
|---|---|---|---|---|---|---|---|
| **Cu** | 3.83 | 13333 | 2256.10 | 134.13 | 4333.3 | 1.88 | 4.95 |
| **Mo** | 0.66 | 11.30 | 3.12 | 1.94 | 3.30 | 1.51 | 3.99 |
| **Zn** | 7.53 | 568 | 69.17 | 24.00 | 103.98 | 2.79 | 12.50 |
| **Co** | 6.00 | 167 | 45.44 | 20.57 | 53.92 | 1.48 | 3.64 |
| **As** | 3.33 | 5960 | 668.46 | 42.00 | 1483.1 | 2.50 | 8.11 |
| **Sb** | 3.33 | 229 | 27.33 | 5.51 | 55.82 | 2.64 | 8.66 |
| **Mg** | 0.06 | 3.07 | 1.06 | 1.06 | 0.78 | 0.69 | 3.06 |
| **Li** | 0.75 | 144 | 22.13 | 10.00 | 32.56 | 2.078 | 6.76 |

Table 2. Pearson's linear correlation coefficient

| | | | | | | | | |
|---|---|---|---|---|---|---|---|---|
| **Cu** | 1.00 | | | | | | | |
| **Mo** | 0.845 | 1.00 | | | | | | |
| **Zn** | 0.573 | 0.440 | 1.00 | | | | | |
| **Co** | 0.872 | 0.734 | 0.504 | 1.00 | | | | |
| **As** | 0.869 | 0.863 | 0.518 | 0.748 | 1.00 | | | |
| **Sb** | 0.816 | 0.869 | 0.464 | 0.653 | 0.963 | 1.00 | | |
| **Mg** | -0.567 | -0.563 | -0.292 | -0.605 | -0.518 | -0.478 | 1.00 | |
| **Li** | 0.631 | 0.444 | 0.388 | 0.811 | 0.541 | 0.389 | -0.543 | 1.00 |
| | Cu | Mo | Zn | Co | As | Sb | Mg | Li |

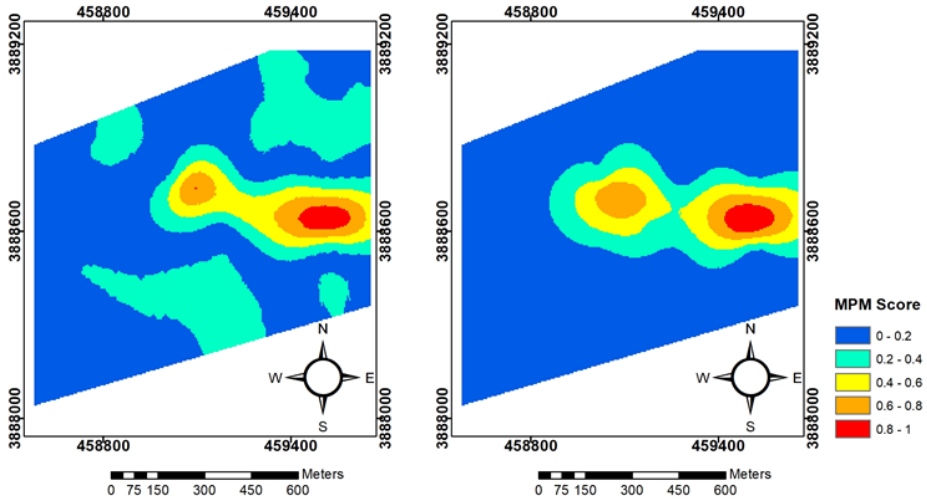


Figure 4. The normalized geochemical indicator layers, (a) Cu concentration, and (b) PC1.

The principal component analysis (PCA), known as a multivariate statistical technique, reduces the dimension of eight lithogeochemical elements. Indeed, it produces principal components (PCs), while the most correlated one with ore mineralization must be searched to be selected as an indicator layer. In this analysis, PC scores are calculated by projection of the original geochemical data onto the PC axes (eigenvectors). The elements of the eigenvector that calculate the PC scores of the original input data are called loadings (or eigenvalues), which are in fact the linear equation coefficients for introducing an eigenvector. The original PCs can be rotated to maximize elements loading in contrast by moving each PC axis to a new position such that the estimates of each variable on the PC axis are near the extremities or near the origin. Therefore, the highest loadings have a value of ± 1 and the lowest ones reach to 0. Table 3 lists eight PCs, in which PC1 with a variation variance of 68.5% was in close adaptation with the Cu mineralization. The PC1 as an indicator layer was portrayed in Fig. 4b.

Table 3. The PC analysis for correlated elements in Cu mineralization, where PC1 was chosen as the main factor

| | PC1 | PC2 | PC3 | PC4 | PC5 | PC6 | PC7 | PC8 |
|---|---|---|---|---|---|---|---|---|
| **Mo** | 0.381 | -0.284 | -0.211 | -0.024 | -0.434 | 0.725 | -0.113 | 0.047 |
| **Cu** | 0.405 | -0.052 | 0.038 | 0.134 | -0.381 | -0.537 | -0.614 | -0.059 |
| **Zn** | 0.262 | -0.055 | 0.869 | -0.4 | 0.026 | 0.104 | 0.039 | -0.016 |
| **Co** | 0.386 | 0.294 | 0.03 | 0.268 | -0.395 | -0.197 | 0.705 | 0.017 |
| **As** | 0.397 | -0.281 | -0.07 | 0.125 | 0.445 | -0.107 | 0.056 | 0.728 |
| **Sb** | 0.374 | -0.438 | -0.143 | 0.039 | 0.4 | -0.097 | 0.183 | -0.666 |
| **Mg** | -0.291 | -0.381 | 0.408 | 0.766 | -0.077 | 0.101 | -0.006 | -0.018 |
| **Li** | 0.303 | 0.641 | 0.084 | 0.378 | 0.382 | 0.324 | -0.273 | -0.139 |
| **% variance** | 68.51 | 11.39 | 8.97 | 6.09 | 2.56 | 1.43 | 0.88 | 0.17 |

*Geophysical layers*

Magnetometry and geoelectric surveys as widespread geophysical tools can provide valuable pieces of information about the types of alteration, rock and ore mineralization, especially in prospecting porphyry–type targets ( Thoman *et al.,* 1998; Clark, 1999; John *et al.,* 2010). Cu–content porphyry deposits are often surrounded by contrasting zones of various alterations around the center of the deposition. Roughly speaking, such alterations are localized by changes of magnetic intensity over their regions, where weak regional magnetic intensity increases sharply over the potassic zone (for presence of iron–oxide content as magnetite), decreases over the sericitic/phyllic zones, and gradually intensifies over the propylitic zone. In analogous to magnetic anomalies, the lowest electrical resistance (Res) and the highest induced polarization (IP) are associated with the sericitic/phyllic alterations that have high sulfide content. Since potassic alteration (as the core of porphyry deposits) is depleted in total sulfide minerals, and the propylitic alteration has low amounts of pyrite minerals, they often correspond to regions with higher electrical resistance and lower polarization (electrical chargeability).

Magnetometry survey was carried out along 28 N–S profiles, where 1077 data were measured at 40–m spacing apart with a station interval of 20 m. The total field magnetic intensity is shown in Fig. 5a. The intensity of the Earth's magnetic field was about 47,680 nT, with an inclination and declination angles of 53.5 and 4.3 degrees, respectively. After removing the regional magnetic field by a polynomial data fitting approach, the reduced–to–pole (RTP) transformation of the residual magnetic data was calculated to remove the inclination effect of the Earth's magnetic field by projecting it at the north pole. In fact, the RTP filter corrects (1) the location of the magnetic anomaly by moving the positive portion of the observed signal over the main causative source of the magnetic anomaly, (2) enhances the intensity of magnetic signal and (3) produces almost a symmetric pattern of an anomaly. The RTP map shown in Fig. 5b indicates that the magnetic field anomalies at the center of the Narbaghi have substantially reduced, which is mainly related to the monzogranite to quartz monzonite units with the phyllic alteration. Porphyry hornblende andesite unit shows an evident dipolar nature of a magnetic anomaly, where no evidences of the Cu–bearing mineralization were observed in geological field operation. Therefore, the indicator layer of the RTP was generated in Fig. 6a as an input layer in the final preparation of the MPM.

To investigate the electrical properties of subsurface layers in the region, 7 time–domain direct current electrical profiles with an electrode spacing of 20 m (increase to a maximum of 40 m) were deployed to measure resistivity and induction polarization at depth. The measurements were carried out using pole–dipole and pole–pole arrays to obtain data from deeper sources. Since the purpose of this research was to generate a 2D MPM map, a horizontal slice was extracted from each inverted electrical model. This depth slice was selected at the center of probable Cu mineralization zone. Fig. 6b and 6c show the indicator maps of the electrical resistivity and chrgability used in the designing of the geospatial database. Both maps indicate that the central part of the prospect area has higher plausibility for Cu mineralization, where the phyllic alteration has occurred within the monzogranite to quartz monzonite units.

**Mineral potential mapping**

In this study, knowledge– and data–driven methods of MPM were used in two sequential phases as a hybrid approach to guide mineral favorability mapping for localizing the main target(s) responsible for Cu–bearing mineralization. The inference network (decision tree) for final preparation of the MPM is presented in Fig. 7.

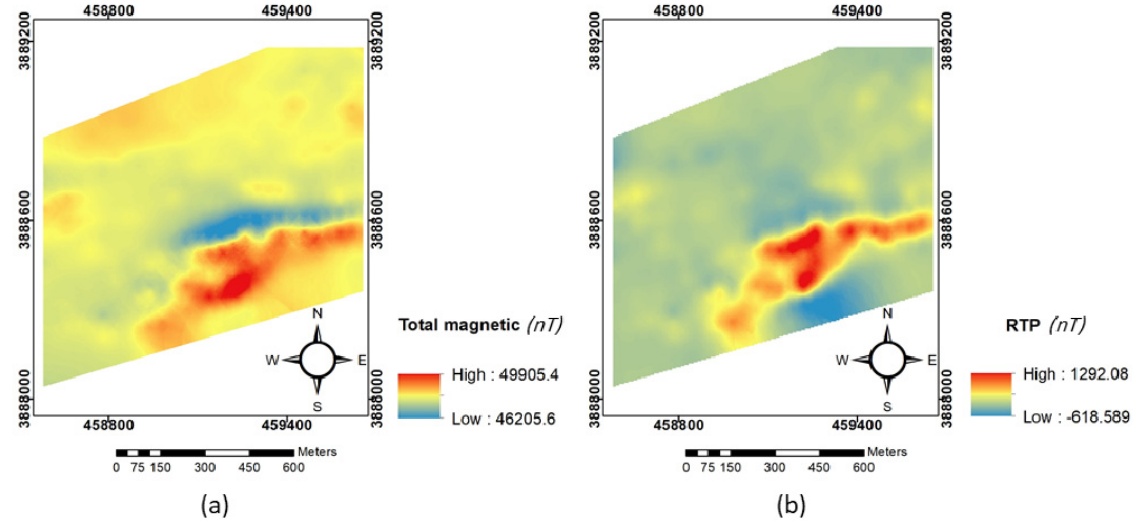


Figure5. The total magnetic field intensity (a) and the RTP magnetic data after removing a regional Earth's magnetic field (b).

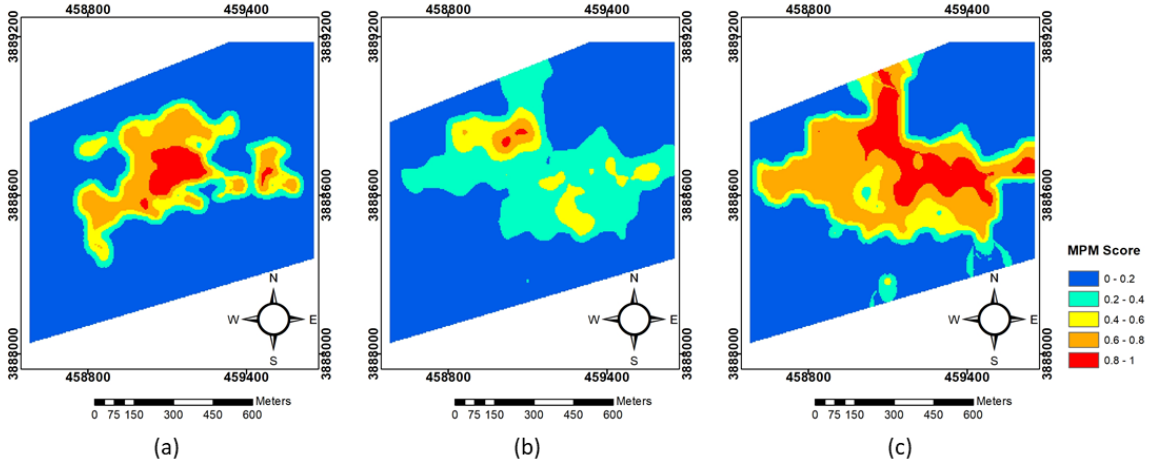


Figure 6. Normalized geophysical indicator layers, (a) magnetometry, (b) IP, and (c) Res.

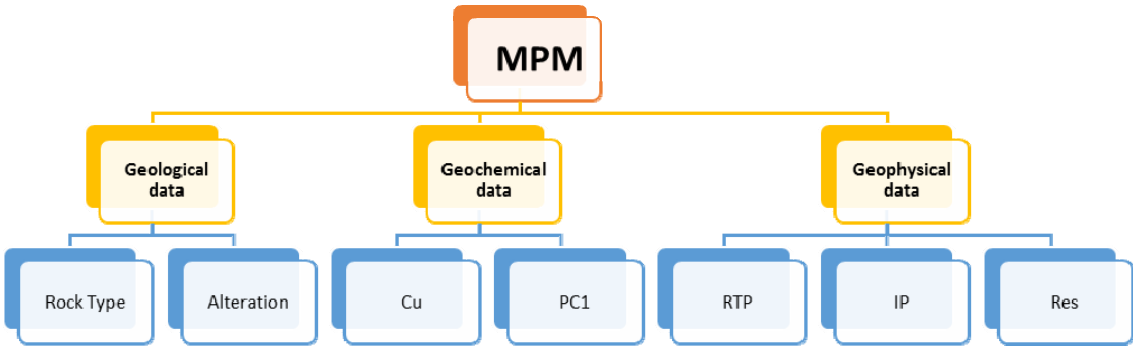


Figure 7. Decision tree flowchart for generating final MPM in Cu exploration.

The proposed knowledge–guided clustering approach performs in two phases, including the knowledge–driven stage and the clustering stage. The procedure of implementing this method has been summarized in Fig. 8. After designating a multidisciplinary geospatial database consisting of aforementioned indicator layers, the knowledge–driven method of fuzzy gamma operator is run for

MPM, where the optimum value of the gamma should be searched in case of accessing to prior information. In first phase, the optimum synthesized fuzzy favorability map is analyzed through a C–A multifractal method to divide this map into some populations which often control by geological and alteration setting of sought mineral target. These populations correspond to the number of clusters which is passed to the second phase of proposed approach. On the basis of this number, a group of clustering algorithms, namely the FCM, KM and SOM are implemented to outline most favorable zones in association with probable Cu mineralization.

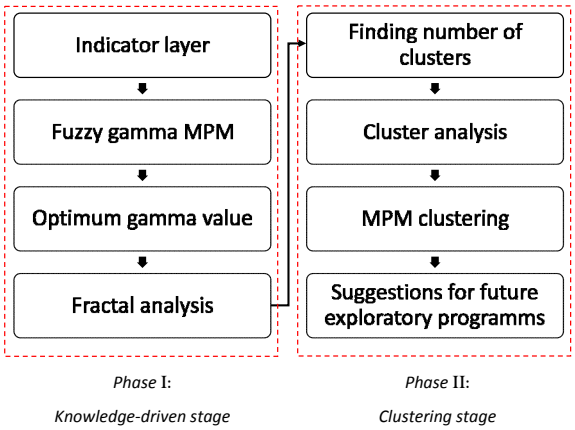


Figure 8. The proposed diagram for the knowledge-driven guided clustering approach in generating MPM.

*Knowledge–driven mapping*

The weights of importance which differentiate superiority of indicator layers to each other were determined through a Delphi method (Dehghan Nayeri, 2018). A group of experts in exploration of porphyry–type ore mineralization was gathered to assign such weights presented in Table 4. The index overlay method as a popular knowledge–driven technique was first utilized to compare its final favorability map with the ones acquired from the fuzzy gamma operator. Figure 9a presents the C–A multifractal curve of the index overlay output, where the prospect region in the North Narbaghi has been divided into five populations. Reclassified favorability map based on the fractal thresholds was portrayed in Fig. 9b, where a distinct potential zone at the center of the area is evident. This zone comprises of two separate sub–zones located over the monzogranite to quartz monzonite units with evidences of the phyllic alteration.

Since the central portions of the North Narbaghi porphyry–Cu mineralization were drilled by 21 vertically boreholes to envisage its mining potential, the productivity index of each drilling was calculated in Table 5 to evaluate the efficiency of the MPM. Whereby the efficiency of each mineral favorability map can be evaluated. The productivity value was calculated from multiplying the Cu concentration (in ppm unit) by its ore thickness (in meter) along each drilling, finally being normalized by the total length of each borehole.

In fact, the productivity index presents the average of the Cu grade along the borehole. Boreholes 10, 13 and 21 were excluded in the MPM efficiency analysis owing to their high uncertainty in grade analysis. Figure 1b has indicated the borehole location. The scatter plot of the productivities versus the values of mineral favorability generated by the index overlay at the locations of boreholes was plotted in Fig. 9c. The Pearson's linear correlation coefficient $(\rho_{Pearson})$ for the fitted linear curve was also calculated equal to 0.47. It is evident that positive correlation must happen when the favorability map is in consistency with the mineralized zones.

In the next step, MPM was performed through implementing the fuzzy gamma operator (FGO). Among all the developed fuzzy operators (An *et al.,* 1991), the FGO, as a combination operator of the fuzzy sum and the product, is the most popular one used in the knowledge–driven MPM.

Table 4. The normalized weight of each criterion in the final copper prospectivity map acquired from a group of geoscientist decision makers

| Layers | Weight | Sub-layer | Weight | Criterion | Weight | Final weights |
|---|---|---|---|---|---|---|
| **Geology** | 0.25 | Surface studies | 1 | Rock type | 0.50 | 0.12500 |
| | | | | Alteration | 0.50 | 0.12500 |
| **Geochemistry** | 0.45 | Lithogeochemical | 1 | Cu | 0.60 | 0.27000 |
| | | | | PC factor | 0.40 | 0.18000 |
| **Geophysics** | 0.3 | Magnetic | 0.35 | RTP | 1.00 | 0.10500 |
| | | Electric | 0.65 | Rs | 0.45 | 0.08775 |
| | | | | IP | 0.55 | 0.10725 |

Table 5. The descriptive of the drilled boreholes with their productivity values.

| Borehole ID | Length (m) | Productivity (ppm) |
|---|---|---|
| **1** | 224.35 | 8.38 |
| **2** | 184.45 | 84.62 |
| **3** | 128.7 | 885.26 |
| **4** | 110.4 | 199.99 |
| **5** | 179.2 | 378.85 |
| **6** | 96.1 | 167.22 |
| **7** | 152.75 | 726.78 |
| **8** | 55 | 107.38 |
| **9** | 52 | 205.02 |
| **10** | 93.4 | 14.68 |
| **11** | 96 | 290.52 |
| **12** | 78 | 382.40 |
| **13** | 126 | 696.23 |
| **14** | 56.6 | 11.02 |
| **15** | 142 | 113.84 |
| **16** | 113 | 119.26 |
| **17** | 71.8 | 732.55 |
| **18** | 54 | 13.44 |
| **19** | 53.5 | 132.45 |
| **20** | 74.8 | 65.51 |
| **21** | 68.3 | 952.46 |

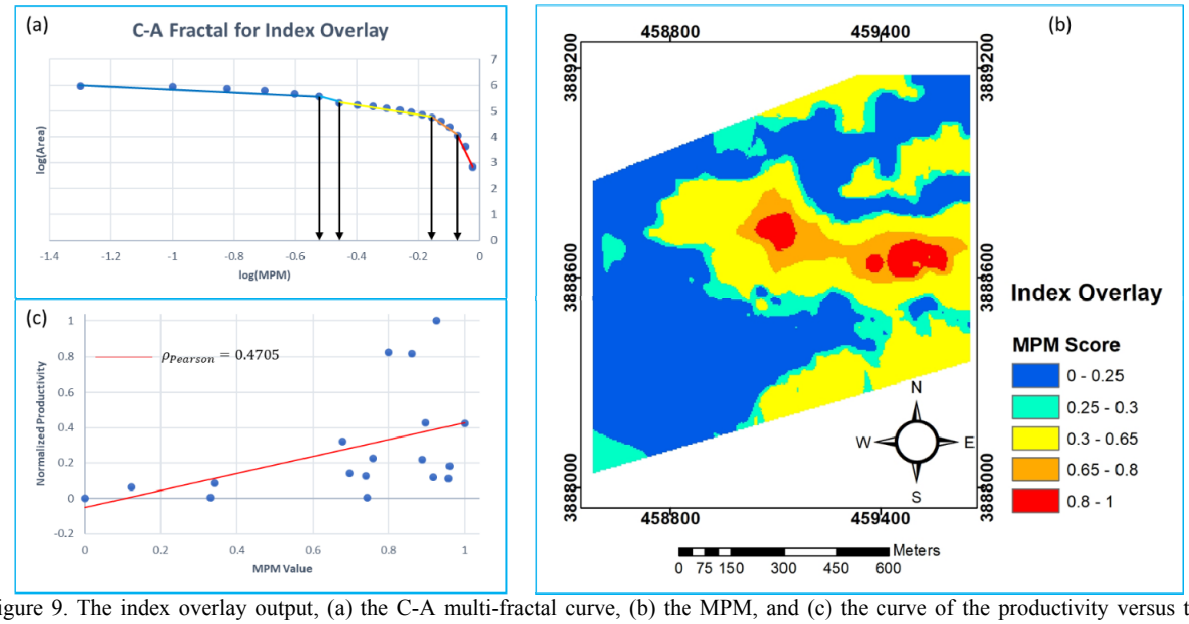


Figure 9. The index overlay output, (a) the C-A multi-fractal curve, (b) the MPM, and (c) the curve of the productivity versus the MPM values at the drilling locations.

Assigning different values of gamma and simple implementation are reasons for its popularity. The optimum value of the gamma is required to be searched by experts among all synthesized fuzzy favorability maps (Nykänen & Salmirinne, 2007; Kashani *et al.,* 2016). According to Nykänen & Salmirinne (2007), the FGO approach method can be utilized to integrate indicator layers without restriction on the selection of the fuzzy gamma value, and it is controlled entirely according to experts' opinion. On the other hand, the FGO is influenced by the pros and cons of both the fuzzy product (more pessimistic than the fuzzy AND) and fuzzy sum (more optimistic than fuzzy OR) operators. By applying this method, MPMs was generated for various gamma values (i.e. $\gamma = 0$, 0.1, 0.2, 0.3, 0.4, 0.5, 0.6, 0.75, 0.9 and 1). Then, to find an optimal gamma, the curves of the productivities versus the MPM values at the drilling locations for each gamma value were plotted in Fig.10. By

comparing the linear regression values obtained, the highest correlation coefficient (0.48) was obtained for γ=1 (Fig. 11c), where this gamma is equivalent to a fuzzy sum product. Therefore, this gamma was selected as an optimum value for MPM (Fig. 11b) since the consistency between the MPM values and the productivity values of drillings is maximum. The C–A multifractal curve of the optimum value has divided the study are into five populations (Fig. 11a), similar to the result of the index overlay with two distinct favorable zones at the center of the North Narbaghi (Fig. 9b).

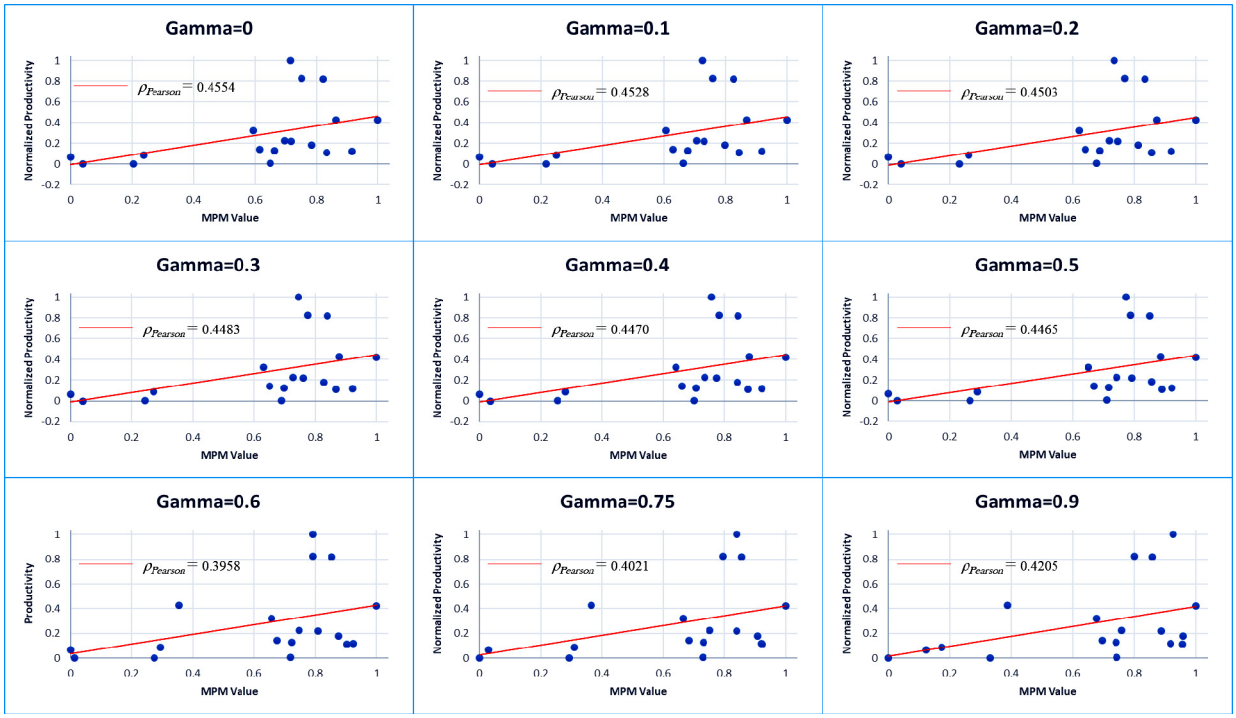


Figure 10. The curve of the Pearson's linear correlation coefficient values calculated from productivity versus the MPM values at the drilling location for various gamma values.

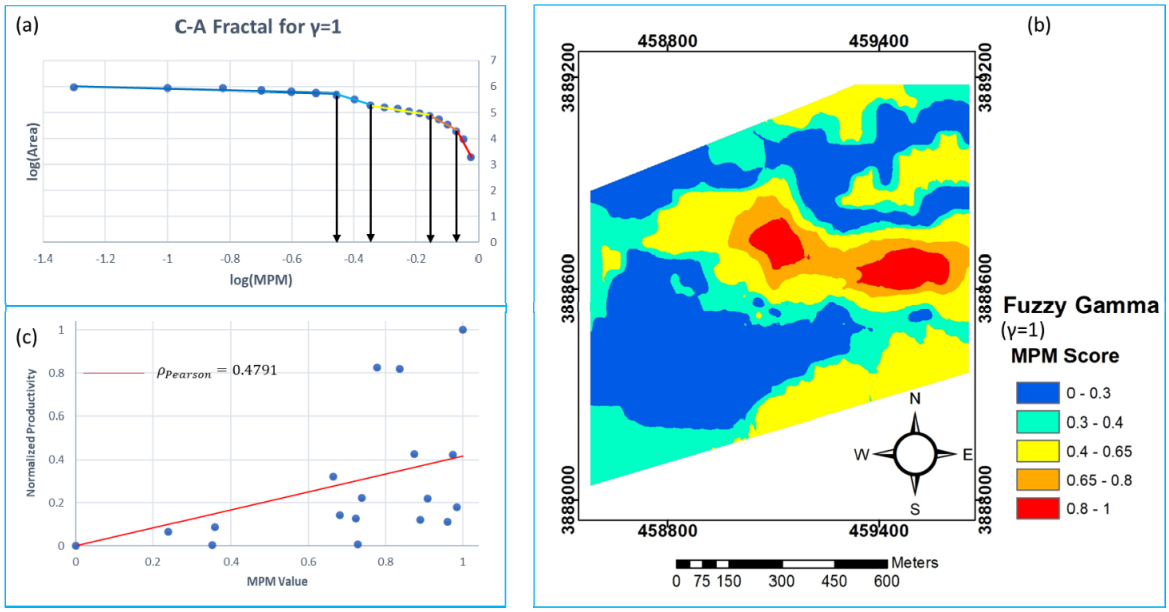


Figure 11. The optimum gamma operator output for generating the MPM, (a) the C-A multi-fractal curve, (b) the MPM and (c) the curve of the productivity versus the MPM values at the drilling locations.

Therefore, we can infer that different knowledge–driven methods will lead to mineral favorability maps with five populations in this region.

*Guided clustering mapping*

According to knowledge driven methods, five populations were generated through running a C–A multifractal curve, where the number of populations was assumed as the optimum number of clusters. Clustering outputs were generated for three algorithms of the FCM, KM, and SOM in a Matlab environment. All generated clustering outputs have highlighted a ribbon of high potential zone (i.e. cluster label 5) in the center of the study area (Figs. 12a, 12b, 12c), whereas this ribbon has been divided into two distinct zones by the FCM method (Fig. 12a) in comparison to the results of the KM and SOM. The results of MPM for such unsupervised data–driven method are in close accordance with the maps of knowledge–based methods, where the central portion of the prospect zone has been localized as the most favorable Cu–bearing zone.

In the knowledge–driven MPMs, experts need to figure out the most realistic relations between the input indicator layers and the final potential map. When each expert assigns the weight of importance to each indicator layer, it may lead to a bias weighting. Therefore, different weights of indicator layers will lead to different maps of the mineral favorability. To tackle this issue in MPM, data–driven methods can be a panacea. Running data–driven methods does not need to determine the weight of each indicator layer, so automatically an MPM can be generated. In cases of no accessing to the training data points for implementing a supervised data–driven method, unsupervised techniques like clustering can be considered. As pointed in this study, a knowledge–guided clustering algorithm was proposed to find the optimum number of clusters in the first phase and then to cluster a multidisciplinary geospatial database in the second phase. Among three clustering methodologies applied in this study, the FCM method could better present the location of the Cu–bearing mineralization.

Figure 13 has depicted a 3D model of the Cu grade where two distinct zones similar to the map generated by the guided FCM clustering are evident.

**Discussion**

A knowledge–guided fuzzy inference approach was applied in this region to investigate the applicability of a fuzzy inference system approach in producing a copper potential map (Barak *et al.,* 2019). The method was implemented in three main stages consisting of (1) fuzzification of input/output data set, (2) designing an inference engine system, and (3) defuzzification of synthesized geospatial indicators. The mineral favorability map was prepared and reclassified into five classes through a multifractal approach. Whereby the synthesized indicator layers demonstrated a Pearson's linear correlation coefficient of 0.44 in recognizing copper mineralization at depth. In addition, the eastern and central portions of the North Narbaghi were proposed as favorable potential zones for further mining operation (Fig. 9b in Barak *et al*., 2019).

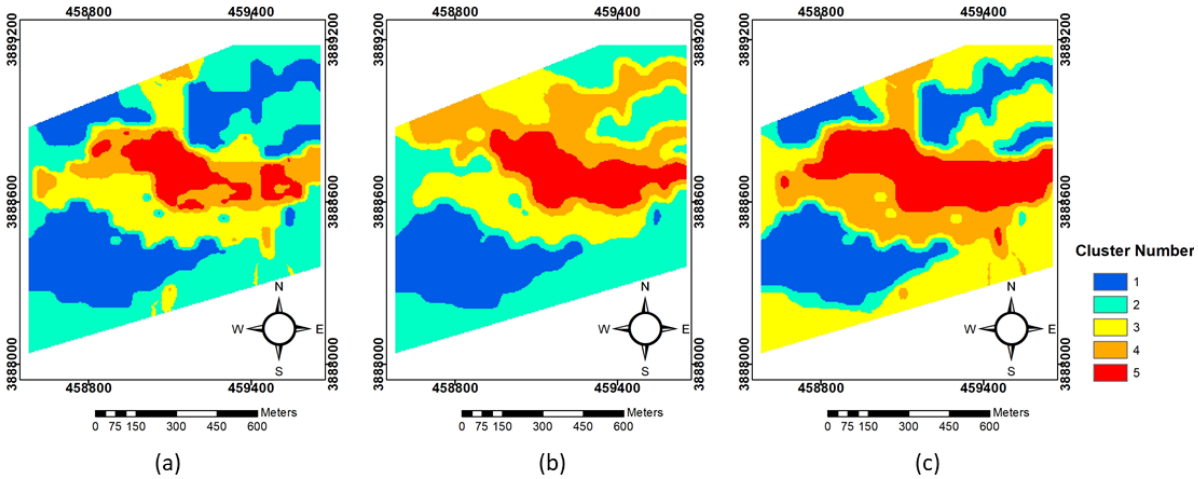


Figure 12. The clustering outputs, (a) FCM, (b) KM, and (c) SOM, where the optimum cluster number was estimated from the fractal analysis of the optimum gamma operator.

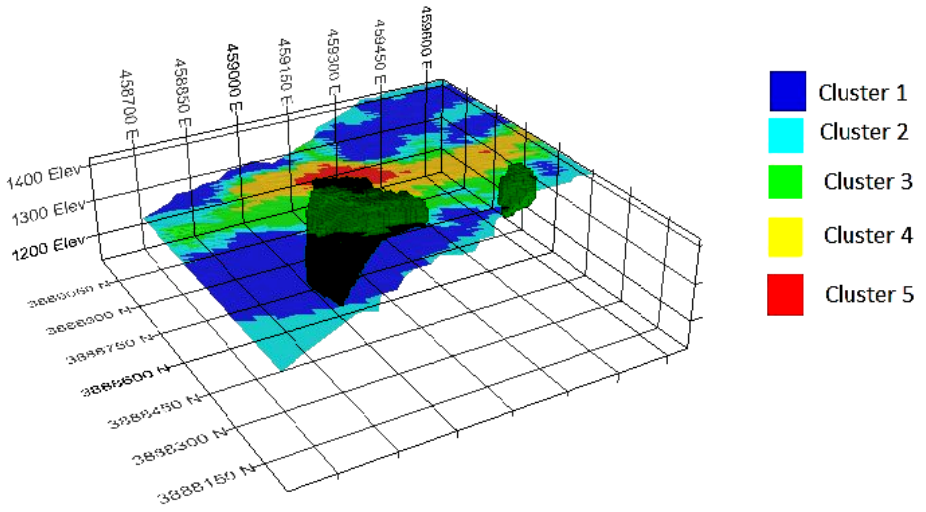


Figure 13. 3D visualization of Cu mineralization overlaid by the FCM map.

Those regions are matched with the ones highlighted in this study (Figs. 11b, 12a, 13).

Since geo–electrical and magnetometry data in this region are available, it is recommended generating a 3D favorability map rather than a 2D map. Note that the 3D indicator layers can be prepared from 3D inversion of geophysical data, while generated and subsequently integrated geophysical models can provide better insights into the geometry of the Cu mineralization. Thus, 3D mineral potential mapping could much better be compared to the drilling results in the deposit–scale cases. Implementation of this suggestion is beyond of the scope of this study.

## Conclusion

A knowledge–guided clustering approach was proposed for mineral favorability mapping, where the optimum number of clusters was determined by a C–A multifractal analysis of a knowledge–based data integration. For this study, the North Narbaghi Cu deposit in Saveh, Markazi province of Iran, was investigated as a deposit–scale case study. Exploratory geospatial datasets comprising of geophysical, geochemical and geological criteria were processed to construct an exploratory decision matrix for MPM. Synthesized mineral favorability map, derived from an optimum fuzzy gamma operator, revealed five clusters in association with the geological setting of the prospect zone. This number of clusters was fixed in running of three clustering algorithms, namely the FCM, KM, and SOM. Note that the FCM output had superiority over other clustering methods in this case study for better determining the geometry of the Cu grade in the North Narbaghi. Therefore, researchers in the field of geospatial data integration for MPM can search the number of populations in the input or synthesized indicator layers, and subsequently assume it as the number of clusters for implementing an unsupervised clustering algorithm.

## Acknowledgements

We thank the Editor–in–Chief of the Geopersia Journal, Dr. Ghasemi–Nejad, and two anonymous referees for reviewing the paper precisely and patiently and for their constructive and valuable comments, which helped us to improve the quality of this work. We also acknowledge the financial support of the University of Tehran for this research under grant number of 30646/1/01.

## References

Abedi, M., Mostafavi Kashani, S.B., Norouzi, G.H., Yousefi, M., 2017. A deposit scale mineral prospectivity analysis: A comparison of various knowledge–driven approaches for porphyry copper targeting in Seridune, Iran. Journal of African Earth Sciences, 128: 127–146.

Abedi, M., Norouzi, G.H., Fathianpour, N., 2015. Fuzzy ordered weighted averaging method: a knowledge–driven approach for mineral potential mapping. Geophys Prospect., 63: 46–477.

Abedi, M., Norouzi, G.H., Fathianpour, N., 2013a. Fuzzy outranking approach: a knowledge–driven method for mineral prospectivity mapping. International Journal of Applied Earth Observation and Geoinformation, 21: 556–567.

Abedi, M., Norouzi, G.H., Torabi, S.A., 2013b. Clustering of mineral prospectivity area as an unsupervised classification approach to explore copper deposit. Arabian Journal of Geosciences, 6: 3601–3613.

Abedi, M., Torabi, S., Norouzi, G.H., 2013c. Application of fuzzy AHP method to integrate geophysical data in a prospect scale, a case study: Seridune copper deposit. Bollettino di Geofisica Teorica ed Applicata, 54: 145–164.

Abedi, M., Norouzi, G.H., 2012. Integration of various geophysical data with geological and geochemical data to determine additional drilling for copper exploration. Journal of Applied Geophysics, 83: 35–45.

Abedi, M., Torabi, S.A., Norouzi, G.H., Hamzeh, M., 2012a. ELECTRE III: A knowledge–driven method for integration of geophysical data with geological and geochemical data in mineral prospectivity mapping. Journal of Applied Geophysics, 87: 9–18.

Abedi, M., Torabi, S.A., Norouzi, G.H., Hamzeh, M., Elyasi, G.R., 2012b. PROMETHEE II: a knowledge–driven method for copper exploration. Computers & Geosciences, 46: 255–263.

Agterberg, F., Bonham–Carter, G.F., 1999. Logistic regression and weights of evidence modeling in mineral exploration: Proceedings Proceedings of the 28th International Symposium on Applications of Computer in the Mineral Industry (APCOM), 483: 490.

Agterberg, F., Bonham–Carter, G.F., Wright, D., 1990. Statistical pattern integration for mineral exploration, Computer applications in resource estimation. Elsevier, 1–21.

An, P., Moon, W., Rencz, A., 1991. Application of fuzzy set theory for integration of geological, geophysical and remote sensing data. Canadian Journal of Exploration Geophysics, 27 (1): 1–11.

Barak, S., Abedi, M., Bahroudi, A., 2019. A knowledge–guided fuzzy inference approach for integrating geophysics, geochemistry and geology data in deposit–scale porphyry copper targeting, Saveh–Iran. Bollettino di Geofisica Teorica e Applicata (in press).

Berberian, M., King, G., 1981. Towards a paleogeography and tectonic evolution of Iran. Canadian Journal of Earth Sciences, 18 (2): 210–265.

Bonham–Carter, G.F., 1994. Geographic information systems for geoscientists–modeling with GIS. Computer methods in the geoscientists, 13: p. 398.

Bonham–Carter, G.F., 1989. Weights of evidence modeling: a new approach to mapping mineral potential. Statistical Applications in the Earth Sciences, 171–183.

Carranza, E.J.M., 2008. Geochemical anomaly and mineral prospectivity mapping in GIS, Elsevier, p. 368.

Carranza, E.J.M., Hale, M., 2002a. Spatial association of mineral occurrences and curvilinear geological features. Mathematical Geology, 34 (2): 203–221.

Carranza, E.J.M., Hale, M., 2002b. Where are porphyry copper deposits spatially localized? A case study in Benguet province, Philippines. Natural Resources Research, 11 (1): 45–59.

Carranza, E.J.M., Hale, M., 2001. Logistic regression for geologically constrained mapping of gold potential, Baguio district, Philippines. Exploration and Mining Geology, 10 (3): 165–175.

Carranza, E.J.M., Mangaoang, J.C., Hale, M., 1999. Application of mineral exploration models and GIS to generate mineral potential maps as input for optimum land–use planning in the Philippines. Natural Resources Research, 8 (2): 165–173.

Chung, C.J.F., Moon, W.M., 1991. Combination rules of spatial geoscience data for mineral exploration. Geoinformatics, 2 (2): 159–169.

Clark, D.A., 1999. Magnetic petrology of igneous intrusions: implications for exploration and magnetic interpretation. Exploration Geophysics, 30 (2): 5–26.

Dehghan Nayeri, R., 2018. Porphyry copper potential mapping in Narbaghi through TOPSIS multi–criteria decision making method: MSc. Thesis in University of Tehran, Iran (published in Persian).

Eberle, D.G., Paasche, H., 2012. Integrated data analysis for mineral exploration: A case study of clustering satellite imagery, airborne gamma–ray, and regional geochemical data suites. Geophysics, 77 (4): B167–B176.

Ghalamghash, J., Fenodi, M., 1998. Geological map of Saveh Quadrangle (scale 1: 100000). Geological survey of Iran.

Harris, D., Zurcher, L., Stanley, M., Marlow, J., Pan, G., 2003. A comparative analysis of favorability mappings by weights of evidence, probabilistic neural networks, discriminant analysis, and logistic regression. Natural Resources Research, 12 (4), 241–255.

John, D., Ayuso, R., Barton, M., Blakely, R., Bodnar, R., Dilles, J., Gray, F., Graybeal, F., Mars, J., McPhee, D., 2010. Porphyry copper deposit model, Chapter B of Mineral deposit models for resource assessment: US Geological Survey Scientific Investigations Report 2010–5070–B.

Kashani, S.B.M., Abedi, M., Norouzi, G.H., 2016. Fuzzy logic mineral potential mapping for copper exploration using multi–disciplinary geo–datasets, a case study in seridune deposit, Iran. Earth Science Informatics, 9 (2): 167–181.

Kazemi, K., Kananian, A., Xiao, Y., Sarjoughian, F., 2019. Petrogenesis of Middle–Eocene granitoids and their Mafic microgranular enclaves in central Urmia–Dokhtar Magmatic Arc (Iran): evidence for interaction between felsic and mafic magmas. Geoscience Frontiers, 10 (2): 705–723.

Mejía–Herrera, P., Royer, J.J., Caumon, G., Cheilletz, A., 2015. Curvature attribute from surface–restoration as predictor variable in Kupferschiefer copper potentials. Natural Resources Research, 24 (3): 275–290.

Mirzaei, M., Afzal, P., Adib, A., Khalajmasoumi, M., Zarifi, A.Z., 2014. Prospection of iron and manganese using index overlay. and fuzzy logic methods in balvard 1: 100,000 sheet, southeastern Iran. Iran J Earth Sci., 6: 1–11.

Moon, W.M., 1990. Integration of geophysical and geological data using evidential belief function. IEEE Transactions on Geoscience and Remote Sensing, 28 (4): 711–720.

Moradi, M., Basiri, S., Kananian, A., Kabiri, K., 2015. Fuzzy logic modeling for hydrothermal gold mineralization mapping using geochemical, geological, ASTER imageries and other geo–data, a case study in Central Alborz, Iran. Earth Science Informatics, 8 (1): 197–205.

Najafi, A., Karimpour, M.H., Ghaderi, M., 2014. Application of fuzzy AHP method to IOCG prospectivity mapping: A case study in Taherabad prospecting area, eastern Iran. International Journal of Applied Earth Observation and Geoinformation, 33: 142–154.

Nykänen, V., 2008. Radial basis functional link nets used as a prospectivity mapping tool for orogenic gold deposits within the Central Lapland Greenstone Belt, Northern Fennoscandian Shield. Natural Resources Research, 17 (1): 29–48.

Nykänen, V., Salmirinne, H., 2007. Prospectivity analysis of gold using regional geophysical and geochemical data from the Central Lapland Greenstone Belt, Finland. Geological Survey of Finland, 44: 251–269.

Paasche, H., Eberle, D.G., 2009. Rapid integration of large airborne geophysical data suites using a fuzzy partitioning cluster algorithm: a tool for geological mapping and mineral exploration targeting. Exploration Geophysics, 40 (3): 277–287.

Pan, G., Harris, D.P., 2000. Information synthesis for mineral exploration (spatial information systems). Oxford University Press, p. 460.

Pazand, K., Hezarkhani, A., 2015. Porphyry Cu potential area selection using the combine AHP–TOPSIS methods: a case study in Siahrud area (NW, Iran). Earth Science Informatics, 8 (1): 207–220.

Porwal, A., Carranza, E., Hale, M., 2003. Artificial neural networks for mineral–potential mapping: a case study from Aravalli Province, Western India. Natural resources research, 12 (3): 155–171.

Porwal, A., Carranza, E., Hale, M., 2004. A hybrid neuro–fuzzy model for mineral potential mapping. Mathematical Geology, 36 (7): 803–826.

Rajabinasab, B., Asghari, O., 2019. Geometallurgical Domaining by Cluster Analysis: Iron Ore Deposit Case Study. Natural Resources Research, 28 (3): 665–684.

Ramazi, H., Jalali, M., 2015. Contribution of geophysical inversion theory and geostatistical simulation to determine geoelectrical anomalies. Studia Geophysica et Geodaetica, 59 (1): 97–112.

Rezaei, S., Lotfi, M., Afzal, P., Jafari, M.R., Meigoony, M.S., 2015. Delineation of Cu prospects utilizing multifractal modeling and stepwise factor analysis in Noubaran 1: 100,000 sheet, Center of Iran. Arabian Journal of Geosciences, 8 (9): 7343–7357.

Sadeghi, B., Khalajmasoumi, M., 2015. A futuristic review for evaluation of geothermal potentials using fuzzy logic and binary index overlay in GIS environment. Renewable and Sustainable Energy Reviews, 43: 818–831.

Sadeghi, B., Khalajmasoumi, M., Afzal, P., Moarefvand, P., 2014. Discrimination of iron high potential zones at the zaghia iron ore deposit, bafq, using index overlay GIS method. Iran J Earth Sci., 6: 91–98.

Shabankareh, M., Hezarkhani, A., 2017. Application of support vector machines for copper potential mapping in Kerman region, Iran. Journal of African Earth Sciences, 128: 116–126.

Shahabpour, J., 2005. Tectonic evolution of the orogenic belt in the region located between Kerman and Neyriz. Journal of Asian Earth Sciences, 24 (4): 405–417.

Singer, D.A., Kouda, R., 1996. Application of a feedforward neural network in the search for Kuroko deposits in the Hokuroku district, Japan. Mathematical Geology, 28 (8): 1017–1023.

Tangestani, M.H., Moore, F., 2002. The use of Dempster–Shafer model and GIS in integration of geoscientific data for porphyry copper potential mapping, north of Shahr–e–Babak, Iran. International Journal of Applied Earth Observation and Geoinformation, 4 (1): 65–74.

Thoman, M.W., Zonge, K.L., Liu, D., 1998. Geophysical case history of North Silver Bell, Pima County, Arizona–a supergene–enriched porphyry copper deposit. Northwest Mining Association, p. 42.

Yousef, M., Kreuzer, O.P., Nykänen, V., Hronsky, J.M.A., 2019. Exploration information systems – A proposal for the future use of GIS in mineral exploration targeting. Ore Geology Reviews, 111: 103005.

Yousefi, M., Carranza, E.J.M., 2016a. Data–driven index overlay and Boolean logic mineral prospectivity modeling in greenfields exploration. Natural Resources Research, 25 (1): 3–18.

Yousefi, M., Carranza, E.J.M., 2016b. Union score and fuzzy logic mineral prospectivity mapping using discretized and continuous spatial evidence values. J. Afr. Earth Sci., 128: 47–60.

Yousefi, M., Carranza, E.J.M., 2015a. Fuzzification of continuous–value spatial evidence for mineral prospectivity

mapping. Computers & Geosciences, 74: 97–109.
Yousefi, M., Carranza, E.J.M., 2015b. Geometric average of spatial evidence data layers: a GIS–based multi–criteria decision–making approach to mineral prospectivity mapping. Computers & Geosciences, 83: 72–79.
Yousefi, M., Carranza, E.J.M., 2015c. Prediction–area (P–A) plot and C–A fractal analysis to classify and evaluate evidential maps for mineral prospectivity modeling. Computers & Geosciences, 79: 69–81.
Zhang, Z., Zuo, R., Xiong, Y., 2016. A comparative study of fuzzy weights of evidence and random forests for mapping mineral prospectivity for skarn–type Fe deposits in the southwestern Fujian metallogenic belt, China. Science China Earth Sciences, 59 (3): 556–572.